Research Square

Preprints are preliminary reports that have not undergone peer review.
They should not be considered conclusive, used to inform clinical practice,
or referenced by the media as validated information.

Intranasal delivery of MSC-derived small extracellular vesicles alleviates motor dysfunction and neuroinflammation in ALS mice and exhibits favorable systemic safety

ShuHan Wang
The First Affiliated Hospital, Sun Yat-sen University
DongXiao Lou
The First Affiliated Hospital, Sun Yat-sen University
SiLin Yu
The First Affiliated Hospital, Sun Yat-sen University
ChanGu Li
The First Affiliated Hospital, Sun Yat-sen University
Qi Sun
The First Affiliated Hospital, Sun Yat-sen University
LongXin Huang
The First Affiliated Hospital, Sun Yat-sen University
YingChun Xie
The First Affiliated Hospital, Sun Yat-sen University
Tian Tian
The First Affiliated Hospital, Sun Yat-sen University
ZhiHui Wang
The First Affiliated Hospital, Sun Yat-sen University
XiaoQing Liu
The First Affiliated Hospital, Sun Yat-sen University
ZhiRou Zhou
The First Affiliated Hospital, Sun Yat-sen University
YuKai Wang
First People's Hospital of Foshan
ChangLin Lian
Guangdong Provincial People's Hospital
QingLing Fu
fuqingl@mail.sysu.edu.cn

The First Affiliated Hospital, Sun Yat-sen University

Research Article

Keywords: Amyotrophic Lateral Sclerosis, MSC-sEVs, Intranasal administration, Neuroinflammation, Neuromuscular junction, Lyophilization, SYF2

Posted Date: November 13th, 2026

DOI: https://doi.org/10.21203/rs.3.rs-11160281/v1

License: This work is licensed under a Creative Commons Attribution 4.0 International License. Read Full License

Additional Declarations: No competing interests reported.

Intranasal delivery of MSC-derived small extracellular vesicles alleviates motor dysfunction and neuroinflammation in ALS mice and exhibits favorable systemic safety

Shu-Han Wang[1#], Dong-Xiao Lou[1#], Si-Lin Yu[1,2#], Chan-Gu Li[1,2], Qi Sun[1,2], Long-Xin Huang[1,2], Ying-Chun Xie[1,2], Tian Tian[1,2], Zhi-hui Wang[1,2], Xiao-Qing Liu[1,2], Zhi-Rou Zhou[1,2], Yukai Wang[3], Chang-Lin Lian[4]*, Qing-Ling Fu[1,2]*

[1]Otorhinolaryngology Hospital, The First Affiliated Hospital, Sun Yat-sen University, 58 Zhongshan Road II, Guangzhou 510080, Guangdong, People's Republic of China. [2]Department of Allergy, The First Affiliated Hospital, Sun Yat-sen University, Guangzhou, People's Republic of China. [3]Department of Neurology, First People's Hospital of Foshan, Foshan, China. [4]Guangdong Provincial Geriatrics Institute, Guangdong Provincial People's Hospital (Guangdong Academy of Medical Sciences), Southern Medical University, Guangzhou, China.

#Shu-Han Wang, Dong-Xiao Lou and Si-Lin Yu contributed equally to this work and share first authorship

*Correspondence:

Dr. Changlin Lian

lianchanglin@hotmail.com

or

Prof. Qing-Ling Fu

Otorhinolaryngology Hospital, The First Affiliated Hospital, Sun Yat-sen University

58 Zhongshan Road II, Guangzhou, Guangdong, 510080, P. R. China

Tel:86-020-87333108; Fax:86-20-87333108;

E-mail: fuqingl@mail.sysu.edu.cn, ORCID: 0000-0002-5969-628X

Abstract

Background Amyotrophic lateral sclerosis (ALS) is a fatal neurodegenerative disease with no curative therapy. Neuroinflammation, glial overactivation, neuromuscular junction (NMJ) damage and neuronal apoptosis are major pathological features of ALS. Mesenchymal stem cell-derived small extracellular vesicles (MSC-sEVs) are neuroprotective and anti-inflammatory and can cross the blood-brain barrier. Here, we investigated the therapeutic efficacy and systemic safety of intranasal MSC-sEVs in ALS mice.

Methods sEVs were isolated from mesenchymal stem cells using anion exchange chromatography, and then lyophilized. The bioactivity of lyophilized MSC-sEVs was validated in a LPS-induced BV2 microglial inflammation model. The $SOD1^{G93A}$ mice were administered by nasal administration, and motor function was assessed by grip strength and rotarod tests. Neuromuscular junction (NMJ) integrity in the gastrocnemius muscle was examined by immunofluorescence. Neuroinflammation and mitochondrial function-related proteins in the spinal cord and cerebral cortex were detected by western blot and immunofluorescence. Public transcriptomic datasets were used to explore the correlation between SYF2 and ALS-related molecular signatures and its regulatory role in mitochondrial gene expression. For safety evaluation, male and female C57BL/6 mice were also treated via intranasal administration, body weight, serum liver and kidney biochemical parameters, and liver and kidney histology were assessed.

Results MSC-sEVs significantly ameliorated motor dysfunction in ALS mice, protected NMJ integrity, inhibited microglial and astrocyte overactivation, and reduced

neuroinflammation. SYF2 was upregulated in ALS patients and correlated with DNA damage-related pathways, while SYF2 silencing upregulated multiple mitochondrial genes enriched in oxidative phosphorylation, suggesting that SYF2 may modulate mitochondrial gene expression in ALS. Safety verification showed that MSC-sEVs caused no adverse effects on mouse growth or liver and kidney function and even improved liver biochemical parameters, showing favorable biosafety.

Conclusions Intranasal MSC-sEVs effectively alleviate neuroinflammation, preserve NMJ integrity and rescue motor impairment in ALS mice, with reliable systemic safety. The preserved bioactivity of lyophilized MSC-sEVs and the involvement of SYF2-mediated mitochondrial regulation support MSC-sEVs as a safe and promising translatable therapeutic candidate for ALS.

Keywords Amyotrophic Lateral Sclerosis, MSC-sEVs, Intranasal administration, Neuroinflammation, Neuromuscular junction, Lyophilization, SYF2

Introduction

Amyotrophic lateral sclerosis (ALS) is a progressive and fatal neurodegenerative disease characterized by the preferential loss of motor neurons in the cerebral cortex, brainstem motor nuclei, and anterior horn of the spinal cord[1]. Disease onset leads to progressive muscle weakness, atrophy, and dysphagia, with death typically resulting from respiratory failure[2]. The disease course typically lasts only 3-5 years[3]. With the aging of the population, the incidence of ALS continues to rise, imposing a heavy burden on patients' families and society[4]. Currently, the clinically approved drugs

riluzole and edaravone offer only modest disease-modifying effects and fail to reverse established neurodegeneration[5]. The newly developed antisense oligonucleotide tofersen, which targets mutant SOD1, is applicable to only ~20% of family ALS cases and shows negligible efficacy in sporadic ALS—the form accounting for the vast majority of patients[6]. Thus, safe and effective therapies are urgently needed.

ALS pathogenesis involves complex interactions across multiple cell types and pathways, and no unified theory fully explains the disease[7]. Glial hyperactivation is a pathological hallmark of ALS, abnormal activation of astrocytes and microglia is a typical feature[8]. Reactive astrocytes cause excitotoxicity, while activated microglia continuously release pro-inflammatory factors, which together form a neuroinflammatory microenvironment that promotes neuronal apoptosis[9, 10]. Mitochondrial dysfunction is also a core mechanism. Motor neurons are highly dependent on mitochondria, and when they are diseased, oxidative phosphorylation is impaired, reactive oxygen species accumulate, and autophagy is abnormal, leading to energy deficiency and a vicious cycle of oxidative stress[11, 12] making mitochondria an important therapeutic target. In addition, degeneration of the neuromuscular junction can occur in the early stage of the disease, manifested as the destruction of the acetylcholine receptor cluster on the postsynaptic membrane and the widening of the synaptic gap resulting in denervation changes[13, 14].

Beyond inflammation and mitochondrial damage, abnormal RNA splicing has emerged as a key pathogenic event in ALS[15]. The splicing factor SYF2, a component of the spliceosome-associated Nineteen Complex, is essential for maintaining normal

pre-mRNA splicing and transcript homeostasis. In ALS, elevated SYF2 expression disrupts RNA processing, promotes TDP-43 aggregation and mislocalization, exacerbates neuronal injury, and triggers apoptotic signaling, making it a promising therapeutic target for diverse forms of ALS[16].

Mesenchymal stem cells (MSCs) are a type of adult stem cells with self-renewal and multi-directional differentiation potential[17]. They exert tissue repair and immune regulation effects through paracrine mechanisms, and the small extracellular vesicles (sEVs) secreted by them are the key carriers mediating this effect[18]. sEVs are nanoscale vesicles with a diameter of 30–200 nm, carrying biological active molecules such as proteins and miRNAs, participating in cell-to-cell communication, and having advantages such as being cell-free, low immunogenicity, and capable of crossing the blood-brain barrier, avoiding the tumor and embolism risks of stem cells transplantation, providing a safe drug delivery route for central nervous system diseases[19, 20]. Among various sources of MSCs, umbilical cord mesenchymal stem cells (UC-MSCs) have outstanding advantages due to their strong proliferation ability, stable genome, and ease of standardized production[21]. MSC-sEVs are rich in anti-inflammatory miRNAs and neurotrophic factors, which can inhibit microglial activation[22], alleviate neuroinflammation[22], and promote the survival of motor neurons[23] and the repair of the neuromuscular junction[24].

Accumulating evidence has demonstrated the therapeutic potential of MSC-sEVs in multiple neurological disorders, including Parkinson's disease[25, 26], Alzheimer's disease[27, 28], ischemic stroke[29], and spinal cord injury[30]. In the context of ALS, while

mesenchymal stem cell-derived extracellular vesicles have shown beneficial effects in preclinical models[31], studies specifically employing MSC-sEVs for ALS remain scarce, with the notable exception of an ongoing clinical trial (NCT06598202) evaluating the safety and preliminary efficacy of intranasal hMSC-sEVs-001 in ALS patients.

Most existing preclinical studies on MSC-sEVs therapy for ALS have relied on invasive administration routes such as intravenous injection, intracerebroventricular infusion, or intrathecal injection, which suffer from low CNS targeting efficiency, poor patient compliance, and unsuitability for long-term repeated administration in chronic progressive ALS[32]. In contrast, intranasal delivery offers a non-invasive, convenient, and repeatable strategy that bypasses the BBB through olfactory and trigeminal nerve pathways, enabling direct targeting of the brain and spinal cord while improving drug bioavailability and reducing systemic side effects[33, 34].

To date, no study has systematically investigated the therapeutic effects of intranasally administered lyophilized MSC-sEVs on motor dysfunction, neuroinflammation, neuromuscular junction integrity, mitochondrial apoptosis, and SYF2-related splicing abnormalities in ALS. Moreover, comprehensive systemic safety evaluations of intranasal MSC-sEVs remain lacking.

Accordingly, this study aimed to investigate the therapeutic effects of intranasally administered lyophilized umbilical cord MSC-sEVs on motor dysfunction, neuroinflammation, NMJ integrity, mitochondrial apoptosis, and SYF2-related splicing abnormalities in $SOD1^{G93A}$ mice. We further systematically evaluated its biosafety in

both male and female C57BL/6 mice.

Methods

Preparation of MSC-sEVs

hUC-MSCs were isolated from Wharton's jelly via the tissue explant method. Briefly, umbilical cords were rinsed with PBS, disinfected in 75% ethanol, and dissected to remove vessels and amniotic membrane. The Wharton's jelly was minced into 3-5 mm^3 fragments, PBS-washed to remove red blood cells, and seeded onto T75 flasks. After 1-2 h attachment at room temperature, complete DMEM/F12 medium (10% FBS, 1% penicillin/streptomycin) was added. Cultures were maintained at 37℃, 5% CO_2 left undisturbed for 5 days (half-medium exchange on day 7). Cells migrated out within 7-10 days and were passaged with 0.25% trypsin at 70%-80% confluence.

MSCs were resuscitated and cultured in 160 cm^2 culture flasks, then transferred to the cell factories for further cultivation. When the cell density reached 80-90%, the serum-free medium was replaced for further culture for 48 hours. The supernatant was collected and sEVs were extracted by anion exchange chromatography after centrifugation at 2660 g for 20 min. The size and concentration of sEVs were detected by Nanoparticle Tracking Analysis (NTA), and the morphology of sEVs was observed by transmission electron microscopy. The exosomal biomarkers of sEVs were identified by Western blot. The purified sEVs were stored at -80℃or mixed with an optimized lyoprotectant, aliquoted into glass vials, and lyophilized. The lyophilized sEVs were stably stored at 4°C for the experiments.

Animal model and MSC-sEV administration

Both C57BL/6 mice and SOD1^{G93A} mice use in this study were maintained in a specific-pathogen-free facility with a 12-h light-dark cycle; room temperature was kept at 22 ± 2 °C and relative humidity at 50–60%. Each cage was supplied with environmental enrichment, and mice had free access to standard chow and autoclaved drinking water. Before any experimental procedures, mice were acclimatized for at least 7 days. All mice were purchased from Kaishi Biotechnology Co., Ltd. (China). General health, body weight, clinical signs and adverse events were monitored routinely during the study. Predefined humane endpoints were used: mice were euthanized if they showed sustained body-weight loss exceeding 20%, inability to access food or water, persistent immobility, or severe clinical deterioration.

Twelve-week-old male SOD1^{G93A} mice were divided into PBS (n=6) and MSC-sEVs (n=8) groups. Lyophilized MSC-sEVs were redissolved using purified water and delivered intranasally at 3×10^9 particles per mouse once every three days, for five doses in total; the PBS group received an equal volume of PBS (Figure 1A). To improve mucosal permeability, 10 μL of hyaluronic acid enzyme was applied intranasally before each dose, followed by sEV administration. Starting at 12 weeks of age, rotarod, grip-strength and body-weight measurements were performed weekly. After the behavioural tests at week 18, mice were anaesthetized with isoflurane (1.5%, 300 mL/min), euthanized by cervical dislocation, and samples were collected. Motor function was the primary outcome and was assessed by grip-strength and rotarod tests. Secondary measures included neuroinflammatory and mitochondrial protein expression,

182 neuromuscular junction (NMJ) integrity, serum biochemistry, liver and kidney
183 histopathology, and transcriptomic pathway analysis.

184 Six-week-old C57BL/6 mice (12 male and 12 female) were studied separately.
185 Within each sex, mice were divided into PBS and lyophilized MSC-sEVs groups (n=6
186 per group). The administration protocol was identical to that used for $SOD1^{G93A}$ mice.
187 Body weight was recorded weekly until week 10. Anaesthesia and euthanasia
188 procedures were the same as described above.

189 No a priori sample-size power calculation was performed because this was a
190 preclinical study. For the $SOD1^{G93A}$ mice experiment, eight mice per group were
191 initially planned. However, two mice in the PBS group died accidentally during
192 isoflurane anaesthesia before intranasal administration, leaving final group sizes of n=6
193 for PBS and n=8 for MSC-sEVs. No surviving animals or data points were excluded
194 from the analysis. These sample sizes were based on our laboratory's previous in vivo
195 experience and the 3Rs principle, with the aim of minimizing animal use.

196 At allocation, mice were assigned to groups using a random-number generator,
197 and group records were retained. The investigators who performed intranasal
198 administration were not blinded because different reagents were used for the two groups.
199 In contrast, behavioural testing, histological and molecular assessments, and statistical
200 analyses were carried out by researchers who remained blinded to group allocation.

201 **Cell culture and treatment**

202 The BV2 cell line was obtained from Professor Shi Lei's laboratory at Jinan
203 University. The BV2 cells were maintained in Dulbecco's modified Eagle's medium

(DMEM) which contained 10 % fetal bovine serum and 2 % penicillin/streptomycin at 37℃ in 5 % CO2. BV2 cells were seeded in 48-well plates and divided into: Control group, LPS group, LPS + MSC-sEVs (-80℃) group, LPS + MSC-sEVs (lyophilized) group. After 6 h of treatment with LPS (100ng/mL) or LPS + MSC-sEVs (2.5×10^9 particles/well), cell culture supernatants were collected to determine IL-6 level.

Grip Strength Test

The grip strength of mice was measured using the grip strength apparatus. The tail base of each mouse was grasped with the index finger and thumb, keeping the trunk horizontal, and the forelimb grip strength was tested. Each mouse was placed horizontally above the grid of the grip strength tester, and its front paws were allowed to grasp the grid naturally. The mouse was then slowly and uniformly pulled away from the grid in the opposite direction until it released the grid, and the maximum grip strength value was automatically recorded. This procedure was repeated 3 times per mouse, with a 6 min interval between each test to avoid muscle fatigue.

Rotarod Test

The motor ability of mice was tested using the rotarod apparatus. The mouse was placed in the center of the rod, and after 10 seconds of adaptation, the equipment was started. The equipment used a uniform acceleration mode: from 6 revolutions per minute to 60 revolutions per minute uniformly accelerated within 300 seconds to test the mouse's adaptation ability and endurance limit. Each mouse repeated the test 3 times, with an interval of 6 min each time. Record the time (dwell time) when the mouse fell off the rod each time. If the mouse jumped off the rod voluntarily, it needed to be

repositioned and the data recorded to ensure the reliability of the experimental results.

Cell culture and treatment

The BV2 cell line (iCell-m011, Cellverse, China) was kindly gifted from Professor Lei Shi's laboratory at Jinan University. The BV2 cells were maintained in Dulbecco's modified Eagle's medium (DMEM) which contained 10 % fetal bovine serum and 2 % penicillin/streptomycin at 37℃ in 5 % CO2. BV2 cells were seeded in 48-well plates and divided into: Control group, LPS group, LPS + MSC-sEVs (-80℃) group, LPS + MSC-sEVs (lyophilized) group. After 6 h of treatment with LPS (100 ng/mL) or LPS + MSC-sEVs (2.5×10^9 particles/well), cell culture supernatants were collected to determine IL-6 level.

Western blot

The brain, L2~L5 lumbar spinal cord, or MSCs were lysed with lysis buffer, centrifuged at 12000 rpm for 15 min, the supernatant was quantified with BCA kit (Beyotime Biotechnology). Then electrophoresis, membrane transfer and closure, then incubated the corresponding membrane at 4 ℃ overnight with the following antibody: anti-GM130 (1:4000, Abcam), anti-Alix (1:8000, Abcam), anti-CD63 (1:2000, Abcam), anti-CD9 (1:2000, Abcam), anti-IL-1β (1:1000, Proteintech), anti-SYF2 (1:2000, Santa Cruz Biotechnology), anti-SOD1 (1:1000, Proteintech), anti-Cytochrome c (1:2000, Proteintech). Washed the membranes with TBST buffer, then incubated with anti-rabbit IgG (1:10000, Abcam) or anti-mouse IgG (1:10000, Abcam) at room temperature for 1 h. Washed the membranes with TBST buffer again. The proteins were visualized by the automatic chemiluminescence imaging and analysis system, and analyzed with Image

J software.

Immunofluorescence

The mouse brain or L2~L5 lumbar spinal cord frozen sections were washed with PBST to remove the OCT embedding agent. After antigen retrieval for 10 min, the sections were blocked with blocking solution for 30 min. They were then incubated overnight at 4°C with the following primary antibodies: anti-IBA1 (1:500, Affinity Biosciences), anti-GFAP (1:500, Proteintech), anti-SOD1 (1:500, Proteintech). Following primary antibody incubation, the sections were washed with PBST and incubated with the corresponding secondary antibodies: goat anti-rabbit IgG H&L Alexa Fluor® 688 (1:500, Abcam) or goat anti-mouse IgG H&L Alexa Fluor® 667 (1:500, Abcam) for 1 hour at room temperature. After washing off the secondary antibodies, the sections were mounted with an anti-fade mounting medium. Finally, images were acquired using a fluorescence microscope.

NMJ staining

Mouse gastrocnemius frozen sections were washed with PBST to remove the OCT embedding agent. After antigen retrieval for 10 min, the sections were blocked with blocking solution for 30 min. They were then incubated with α-BTX (600 nM) overnight at 4°C. Following incubation, the sections were rinsed with PBST and mounted with an anti-fade mounting medium. Finally, images were acquired under a fluorescence microscope.

Biochemical index detection

Mouse whole blood was collected via eyeball extraction and allowed to clot at

room temperature for 1 hour. Serum was then separated by centrifugation at 3,000 rpm for 15 min and stored for subsequent analysis. Strictly following the manufacturer's instructions for the corresponding biochemical assay kits, the serum levels of aspartate aminotransferase (AST), alanine aminotransferase (ALT), blood urea nitrogen (BUN), enzymatic creatinine (ECre3), and uric acid (UA) were measured. The absorbance values for each index were recorded using an automatic biochemical analyzer, and the corresponding concentrations were calculated based on the standard curve.

ELISA

Microplates were coated with IL-6 capture antibody diluted in coating buffer and incubated overnight at 4°C. After three PBST washes, wells were blocked for 1–2 h at RT, then the blocking solution was removed without washing. Standards and samples were added in duplicate, along with blanks and controls, and incubated for 2 h at RT. After 3–5 PBST washes, detection antibody was applied for 1 h at RT, followed by HRP-conjugated secondary antibody for 1 h in the dark, with 5 washes after each step. Color was developed with TMB substrate for 5–30 min in the dark until the desired intensity appeared. The reaction was stopped with 50 μL stop solution, and the absorbance was read at 450 nm. Sample concentrations were calculated from the standard curve.

HE staining

Paraffin sections of mouse liver and kidney were prepared and subjected to gradient dehydration. The sections were then immersed in hematoxylin solution for 6 min, followed by a 20 min rinse under running water. After differentiation in 1%

hydrochloric acid in ethanol for 1 second, the sections were rinsed again in running water for 20 min. Subsequently, the sections were counterstained in 1% alcoholic eosin solution for 10 seconds. Following staining, the sections underwent gradient dehydration, were cleared, and then mounted with neutral resin. Finally, images were observed and captured under a microscope.

Data Sources

The RNA-Seq data used in this study were all obtained from processed count matrices provided by NCBI GEO. No raw sequencing data alignment or expression quantification was performed in this study. Postmortem brain RNA-Seq data from the NYGC ALS Consortium were obtained from the GEO dataset GSE153960, which contains samples from ALS patients and Non-Neurological controls. Cell model RNA-Seq data were obtained from the GEO dataset GSE218079. This dataset contains human induced motor neurons (iMNs) differentiated from C9orf72-mutant ALS patient tissue, and the treatment groups included a scrambled siRNA control group and an SYF2 siRNA group.

Differential Expression Analysis

Differential expression analysis was performed using R and the DESeq2 package. The Wald test was used to assess differences in gene expression, and P values were corrected for multiple testing using the Benjamini-Hochberg method. Genes with $|\log2FC| > 1$ and $Padj < 0.05$ were considered differentially expressed.

GSVA Pathway Scoring

GSVA was used to calculate sample-level pathway scores. The input data were the count matrices provided by GEO, and 23 DNA damage-related pathway sets were collected for scoring. ALS samples were divided into SYF2high and SYF2low groups according to the median SYF2 expression level. Pathway scores related to DNA damage were compared between the two groups, and $P < 0.05$ was considered statistically significant.

Enrichment Analysis and GSEA

Pathway enrichment analysis was performed on genes significantly upregulated after SYF2 silencing, and P values were corrected using the Benjamini-Hochberg method. GSEA was used to evaluate the enrichment of oxidative phosphorylation and related nervous system disease gene sets after SYF2 silencing. Enrichment significance was determined based on the normalized enrichment score (NES), nominal P value, and FDR q value. Padj < 0.05 or FDR < 0.05 was considered statistically significant.

Statistical Analysis

Data were presented as mean ± SD and were analyzed using GraphPad Prism 9.0.0. Behavioral data were analyzed by two-way ANOVA followed by Bonferroni post hoc test. Two-group comparisons were performed using using an unpaired t-test. Multiple-group comparisons were performed by one-way ANOVA followed by Tukey's post hoc test. $P < 0.05$ was considered statistically significant.

Results

Extraction and Characterization of MSC-sEVs

MSC supernatants were extracted from umbilical cord-derived MSCs using an anion exchange chromatography method (Fig. 1A). NTA analysis and transmission electron microscopy results showed that the sEVs were uniform in size and presented typical cup-shaped or spherical vesicle structures, with complete lipid bilayer membranes (Fig. 1B-C). Western blot analysis confirmed that sEVs were positive for exosomal biomarkers such as Alix, CD63 and CD9, and negative for the cis-Golgi matrix protein GM130, indicating negligible contamination by cellular organelles. The expression intensity of Alix was weaker than that of the cells, which was consistent with the characteristic expression pattern of exosomes (Fig. 1D). To evaluate the long-term storage stability of lyophilized sEVs, MSC-sEVs were stored in liquid or lyophilized form at -80°C and 4°C for one month. The bioactivity of MSC-sEVs was then assessed in an LPS-induced BV2 microglial inflammation model. ELISA results showed that lyophilized MSC-sEVs reduced IL-6 level more effectively than liquid-stored MSC-sEVs (Fig. 1E). These characterization results confirmed successful MSC-sEV extraction and demonstrated that lyophilized sEVs retained superior bioactivity.

Intranasal MSC-sEVs rescues motor function and protects NMJ in SOD1^{G93A} mice

Lyophilized MSC-sEVs were administered intranasally to SOD1^{G93A} mice to evaluate their effects on improving motor function. We observed that at week 16, the body weight ratio was significantly higher in the MSC-sEVs group than in controls, but this difference disappeared by week 17, with no statistical difference between groups thereafter (Fig. 2B). And the grip strength and rod-turning experiments showed that

MSC-sEVs could significantly delay the decline in grip strength and rod-turning latency of SOD1^{G93A} transgenic mice and effectively improve their motor dysfunction (Fig. 2C-D). The α-BT staining results indicated that after administration of MSC-sEVs, the neuromuscular junction of the gastrocnemius muscle of SOD1^{G93A} transgenic mice was more intact. These results indicate that intranasal delivery of MSC-sEVs can protect the neuromuscular junction integrity of SOD1^{G93A} transgenic mice and improve their motor dysfunction.

MSC-sEVs alleviate spinal nerve inflammation in SOD1^{G93A} mice and regulate the levels of injury-related proteins

The Western blot results showed that MSC-sEVs could significantly down-regulate the expression of pro-inflammatory factor IL-1β, splicing-related factor SYF2, and apoptosis-related protein Cytochrome C in the spinal cord of SOD1^{G93A} mice (Fig. 3B-E). The immunofluorescence results further indicated that MSC-sEVs could inhibit the excessive activation of spinal astrocytes and microglia (Fig. 3F). These results suggest that MSC-sEVs may exert neuroprotective effects on spinal tissue by inhibiting the neuroinflammatory response mediated by glial cells, reducing the release of pro-inflammatory factors, and alleviating abnormal splicing-related damage and activation of the mitochondrial apoptotic pathway, thereby delaying the pathological progression of ALS.

MSC-sEVs inhibit neuroinflammation in the cerebral cortex of SOD1^{G93A} mice and regulate the levels of injury-related proteins

The results of Western blot showed that MSC-sEVs could significantly down-

regulate the expression of pro-inflammatory factor IL-1β, splicing regulatory factor SYF2, pathogenic mutant protein SOD1, and mitochondrial apoptosis key protein Cytochrome C in the cerebral cortex of $SOD1^{G93A}$ mice (Fig. 4B-E). Moreover, the results of immunofluorescence indicated that MSC-sEVs could inhibit the excessive activation of microglia and the expression of SOD1 in the cerebral cortex of $SOD1^{G93A}$ mice, alleviate central glial hyperplasia (Fig. 4F). These results suggest that MSC-sEVs can target both the cerebral cortex and spinal cord, two major central lesion areas. On one hand, it can reduce abnormal glial activation and the release of inflammatory factors to alleviate central nervous inflammation and improve abnormal RNA splicing disorder; on the other hand, it can down-regulate the accumulation of pathogenic mutant SOD1 protein, inhibit the activation of the mitochondrial apoptosis pathway, and reduce neuronal damage. Thus, MSC-sEVs can improve the pathological damage of the central nervous system in ALS mice through multiple mechanisms and multiple targets, effectively delaying the disease progression.

SYF2 correlates with ALS-associated molecular signatures and modulates mitochondrial-related pathways

Based on our analyses of public transcriptomic datasets (GSE218079), SYF2 expression was significantly elevated in patients with ALS (Fig. 5A). Notably, this upregulation was accompanied by higher activation scores for DNA damage-related signaling pathways within the SYF2-high subgroup (Fig. 5B). To determine whether SYF2 functionally underlies these molecular phenotypes, we performed SYF2 knockdown and observed consistent upregulation of a panel of mitochondrial genes,

including ND1, ND5, ND6, ATP6, ATP8, and CYTB (Fig. 5C). Pathway enrichment of genes differentially upregulated following SYF2 silencing revealed prominent enrichment in oxidative phosphorylation alongside sEV several nervous-system-disease-associated pathways (Fig. 5D-E), suggesting that SYF2 may modulate mitochondrial gene expression in the context of ALS.

Safety Evaluation of MSC-sEVs

We next evaluated the in vivo safety of intranasal MSC-sEVs in male and female C57BL/6 mice by monitoring body weight, serum liver/kidney biochemical parameters, and histopathology of liver and kidney tissues. The results showed that the body weight of mice in each group increased steadily over time, with no significant differences between groups (Fig. 6B and 7B). The serum biochemical test results indicated that compared with the control group, the levels of AST, BUN, ECre3, and UA in the MSC-sEVs administration group did not show significant changes (Fig. 6C and E-G, 7C and E-G), but the expression level of ALT decreased significantly (Fig. 6D and 7D), suggesting a potential hepatoprotective effect of MSC-sEVs. The HE staining of liver and kidney tissues further indicated that the liver and kidney tissue structures of both groups of mice were intact, with normal morphology, and the degree of inflammatory infiltration was mild with no significant differences between groups (Fig. 6H and 7H). These results collectively confirm that intranasal administration of MSC-sEVs poses no detectable toxicity to mouse growth, liver/kidney function, or tissue morphology. Notably, the observed reduction in ALT levels suggests a potential hepatoprotective effect, further supporting the favorable safety profile of MSC-sEVs for future clinical

application.

Discussion

ALS is a rapidly progressing and highly fatal neurodegenerative disease[35]. The current clinical drugs can only slightly delay the disease course but cannot reverse the neurodegenerative damage[36]. Moreover, the applicable population for targeted drugs is limited. In this study, intranasal administration of MSC-sEVs effectively improved motor performance, mitigated neuroinflammation, and protected NMJ integrity in $SOD1^{G93A}$ mice. Concurrent safety assessments in both male and female C57BL/6 mice confirmed the absence of overt toxicity.

Most preclinical studies on MSC-sEVs therapy for ALS have relied on invasive routes such as intracerebroventricular or intravenous injection[37, 38]. These approaches, however, pose challenges in patient compliance, delivery consistency, and long-term safety, especially when repeated dosing is required[39]. Intranasal administration offers a non-invasive, patient-friendly alternative that can bypass the blood–brain barrier and deliver therapeutics directly to the central nervous system via the olfactory and trigeminal pathways[40-42]. This route is particularly attractive for chronic neurodegenerative diseases like ALS, where long-term intervention is essential[31]. Our study thus introduces a clinically more feasible delivery route for MSC-sEVs therapy, facilitating its future translation to the clinic[34].

MSC-sEVs was purified by anion exchange chromatography and verified through TEM, NTA and Western blot experiments. The morphology, particle size characteristics

444 and specific marker expression of the extracted MSC-sEVs all met the criteria for
445 exosome identification, and the sample purity and reliability were good. Current
446 research indicates that lyophilization of EVs can significantly enhance storage stability,
447 eliminate the need for ultra-low temperature cold chain, enable long-term preservation,
448 and effectively maintain the vesicle structure, markers, and biological activity[43, 44].
449 Therefore lyophilization was employed to achieve stable storage of MSC-sEVs at 4°C,
450 effectively solving the limitations of traditional vesicle storage and transportation, and
451 enhancing its clinical translation value. Importantly, our bioactivity assessment in LPS-
452 stimulated BV2 microglia confirmed that lyophilized MSC-sEVs retained—and even
453 outperformed—the anti-inflammatory efficacy of liquid-stored sEVs in reducing IL-6
454 secretion. This finding not only validates the feasibility of lyophilization as a long-term
455 preservation strategy but also ensures that the therapeutic benefits observed in vivo are
456 not compromised by the freeze-drying process.

457 The behavioral and immunofluorescence staining results of $SOD1^{G93A}$ mice
458 showed that intranasal delivery of MSC-sEVs could significantly improve the motor
459 dysfunction of $SOD1^{G93A}$ mice. NMJ damage, a hallmark of ALS pathology, directly
460 contributes to motor dysfunction[45]. MSC-sEVs effectively preserved NMJ integrity in
461 $SOD1^{G93A}$ mice.

462 Central nervous inflammation, abnormal accumulation of SOD1 protein and
463 mitochondrial apoptosis are the key driving factors of ALS progression[46, 47]. MSC-
464 sEVs significantly inhibited microglial and astrocyte overactivation in both the spinal
465 cord and cerebral cortex, reduced IL-1β expression, and attenuated the

neuroinflammatory microenvironment. At the same time, MSC-sEVs could reduce the accumulation of abnormal SOD1 protein in brain tissue, regulate the expression of splicing factor SYF2 and key protein Cytochrome C of mitochondrial apoptosis, inhibit the activation of the mitochondrial apoptosis pathway, reduce neuronal degeneration, and exert central nervous protection through multiple targets and pathways. Beyond inflammation and mitochondrial apoptosis, our bioinformatic and experimental analyses identified SYF2 as a potential molecular target of MSC-sEVs action. Analysis of public transcriptomic datasets revealed that SYF2 expression was significantly elevated in ALS patients and correlated with higher activation scores of DNA damage-related pathways. In cellular models, SYF2 silencing upregulated a panel of mitochondrial-encoded genes—including ND1, ND5, ND6, ATP6, ATP8 and CYTB, with pathway enrichment predominantly mapping to oxidative phosphorylation. These findings suggest that SYF2 may function as a negative regulator of mitochondrial gene expression in the ALS context. Given that MSC-sEVs treatment downregulated SYF2 expression in both the spinal cord and cerebral cortex of $SOD1^{G93A}$ mice, it is plausible that the neuroprotective effects of MSC-sEVs are partly mediated through relief of SYF2-associated mitochondrial dysfunction and splicing abnormalities. This mechanistic insight aligns with previous reports linking SYF2 suppression to mitigation of neurodegeneration in diverse ALS models[16], and further expands the therapeutic rationale for MSC-sEVs in targeting ALS-associated molecular pathways. While our data reveal a correlation between SYF2 downregulation and therapeutic efficacy, the upstream regulatory mechanisms by which MSC-sEVs modulates SYF2 expression

remain to be elucidated, representing a key direction for future investigation.

Preclinical safety is a key prerequisite for the transformation and application of biological agents[48]. This study used male and female C57BL/6 mice to evaluate the safety of intranasal delivery of MSC-sEVs. The experimental results showed that intranasal delivery of MSC-sEVs had no adverse effects on the body weight and liver and kidney functions of mice, and no obvious pathological damage was observed in liver and kidney tissues. The decrease in ALT level after administration indicated that MSC-sEVs had a certain positive regulatory effect on the liver function homeostasis.

In summary, our study demonstrates that intranasal MSC-sEVs not only ameliorates motor dysfunction and neuroinflammation via multiple pathways, but also that its lyophilized formulation retains full bioactivity. The involvement of SYF2-mediated mitochondrial regulation provides a novel mechanistic link between MSC-sEVs therapy and ALS pathogenesis, warranting further investigation into the upstream regulatory mechanisms of SYF2 modulation by sEVs.

Conclusions

Collectively, our findings revealed that intranasally delivered MSC-sEVs potently mitigates neuroinflammation, protects NMJ structure, and improves motor function in ALS mice, with no obvious systemic toxicity. This noninvasive therapeutic strategy highlights MSC-sEVs as a safe and clinically translatable candidate for ALS intervention.

Acknowledgments

Thanks the drawing tools provided by Figuredraw. The authors declare that they have

not used AI-generated work in this manuscript.

Abbreviations

ALS Amyotrophic lateral sclerosis

BBB Blood-brain barrier

CNS Central nervous system

α-BTX α -bungarotoxin

NMJ Neuromuscular junction

MSCs Mesenchymal stem cells

sEVs Small extracellular vesicles

Author contributions

SW helped in collection and assembly of data and manuscript writing. DL and SY helped data analysis, discussion and manuscript writing. CL, QS, LH, YX, TT, ZW, XL and RZ helped in the collection of data. YW collected human umbilical cord tissues. CL helped in concept and design, data analysis. QF helped in concept and design, data analysis, manuscript writing, and final approval of the manuscript. All authors contributed to the article and approved the submitted version.

Funding

This work was supported by National Key R&D Program of China (No. 2022YFA1104900), the National Natural Science Foundation of China (Nos. 82571286), and the Key R&D Program of Guangzhou (Nos.2023B03J1233).

Declarations

Ethics approval and consent to participant

The human umbilical cords were obtained from the First People's Hospital of Foshan. Written informed consent was acquired from all healthy adult pregnant donors prior to umbilical cord tissue collection. This study was approved by the Institutional Ethics Committee of First People's Hospital of Foshan (Approval number: Research Ethics Review No. (2022) 12; Approval date: 28 January 2022). All animal experiments were performed in accordance with the ARRIVE guidelines and the national guidelines for the care and use of laboratory animals. The animal study protocol was approved by the Institutional Animal Ethics Committee, Greater Bay Area Institute of Precision Medicine (Guangzhou) (Approval number: IPMGBA-25-0027); Approval date: 2 September 2025.

Availability of data and materials

Public transcriptomic datasets analysed in this work were obtained from the Gene Expression Omnibus (GEO) repository, with accession numbers GSE218079 and GSE153960. All other raw experimental data generated in our study are available from the corresponding author upon reasonable request.

Consent for publication

Not applicable.

Competing interests

The authors declare no conflicts of interest in this work.

References

[1] Desai AB, Agarwal A, Mohamed AS, et al. Motor Neuron Diseases and Central Nervous System Tractopathies: Clinical-Radiologic Correlation and Diagnostic Approach. Radiographics. 2025;45(1):e240067.

[2] Müller KJ, Schmidbauer ML, Schönecker S, et al. Diagnostic accuracy and confounders of vagus nerve ultrasound in amyotrophic lateral sclerosis-a single-center case series and pooled individual patient data meta-analysis. J Neurol. 2024;271(9):6255-6263.

[3] Baloh RH, Johnson JP, Avalos P, et al. Transplantation of human neural progenitor cells secreting GDNF into the spinal cord of patients with ALS: a phase 1/2a trial. Nat Med. 2022;28(9):1813-1822.

[4] Berry JD, Blanchard M, Bonar K, et al. Epidemiology and economic burden of amyotrophic lateral sclerosis in the United States: a literature review. Amyotroph Lateral Scler Frontotemporal Degener. 2023;24(5-6):436-448.

[5] Elmansy MF, Reidl CT, Rahaman M, Özdinler PH, Silverman RB. Small molecules targeting different cellular pathologies for the treatment of amyotrophic lateral sclerosis. Med Res Rev. 2023;43(6):2260-2302.

[6] Ruffo P, Traynor BJ, Conforti FL. Advancements in genetic research and RNA therapy strategies for amyotrophic lateral sclerosis (ALS): current progress and future prospects. J Neurol. 2025;272(3):233.

[7] Ince PG, Highley JR, Kirby J, et al. Molecular pathology and genetic advances in amyotrophic lateral sclerosis: an emerging molecular pathway and the significance of glial pathology. Acta Neuropathol. 2011;122(6):657-671.

[8] Calafatti M, Cocozza G, Limatola C, et al. Microglial crosstalk with astrocytes and immune cells in amyotrophic lateral sclerosis. Front Immunol. 2023;14:1223096.

[9] You J, Youssef MMM, Santos JR, et al. Microglia and Astrocytes in Amyotrophic Lateral Sclerosis: Disease-Associated States, Pathological Roles, and Therapeutic Potential. Biology (Basel). 2023;12(10):1307.

[10] Valori CF, Sulmona C, Brambilla L, Rossi D. Astrocytes: Dissecting Their Diverse Roles in Amyotrophic Lateral Sclerosis and Frontotemporal Dementia. Cells. 2023;12(11):1450.

[11] Yipeng X, Guiqian W, Qiaochu Z, et al. Molecular mechanisms by which mitochondrial dysfunction drives neuromuscular junction degeneration in amyotrophic lateral sclerosis. Neurobiol Dis. 2025;216:107103.

[12] Gao Y, Wang C, Jiang D, et al. New insights into the interplay between autophagy and oxidative and endoplasmic reticulum stress in neuronal cell death and survival. Front Cell Dev Biol. 2022;10:994037.

[13] Margotta C, Fabbrizio P, Ceccanti M, et al. Immune-mediated myogenesis and acetylcholine receptor clustering promote a slow disease progression in ALS mouse models. Inflamm Regen. 2023;43(1):19.

[14] Gelon PA, Dutchak PA, Sephton CF. Synaptic dysfunction in ALS and FTD: anatomical and molecular changes provide insights into mechanisms of disease. Front Mol Neurosci. 2022;15:1000183.

[15] Nikom D, Zheng S. Alternative splicing in neurodegenerative disease and the promise of RNA therapies. Nat Rev Neurosci. 2023;24(8):457-473.

[16] Linares GR, Li Y, Chang WH, et al. SYF2 suppression mitigates neurodegeneration in models of diverse forms of ALS. Cell Stem Cell. 2023;30(2):171-187.e14.

[17] Xia P, Shi Y, Wang X, Li X. Advances in the application of low-intensity pulsed ultrasound to mesenchymal stem cells. Stem Cell Res Ther. 2022;13(1):214.

[18] Peng YQ, Deng XH, Xu ZB, Wu ZC, Fu QL. Mesenchymal stromal cells and their small extracellular vesicles in allergic diseases: From immunomodulation to therapy. Eur J Immunol. 2023;53(10):e2149510.

[19] Zhou X, Huang J, Zhang D, Qian Z, Zuo X, Sun Y. Small extracellular vesicles: the origins, current status, future prospects, and applications. Stem Cell Res Ther. 2025;16(1):184.

[20] Li M, Fang F, Sun M, Zhang Y, Hu M, Zhang J. Extracellular vesicles as bioactive nanotherapeutics: An emerging paradigm for regenerative medicine. Theranostics. 2022;12(11):4879-4903.

[21] Meng M, Zhang WW, Chen SF, Wang DR, Zhou CH. Therapeutic utility of human umbilical cord-derived mesenchymal stem cells-based approaches in

pulmonary diseases: Recent advancements and prospects. World J Stem Cells. 2024;16(2):70-88.

[22] Figueroa-Valdés AI, Luz-Crawford P, Herrera-Luna Y, et al. Clinical-grade extracellular vesicles derived from umbilical cord mesenchymal stromal cells: preclinical development and first-in-human intra-articular validation as therapeutics for knee osteoarthritis. J Nanobiotechnology. 2025;23(1):13.

[23] Nakazaki M, Lankford KL, Yamamoto H, Mae Y, Kocsis JD. Human mesenchymal stem-derived extracellular vesicles improve body growth and motor function following sEVsere spinal cord injury in rat. Clin Transl Med. 2023;13(6):e1284.

[24] Chen J, Zhu Y, Gao H, et al. HucMSCs Delay Muscle Atrophy After Peripheral Nerve Injury Through Exosomes by Repressing Muscle-Specific Ubiquitin Ligases. Stem Cells. 2024;42(5):460-474.

[25] Huang W, Zhang T, Li X, et al. Intranasal Administration of Umbilical Cord Mesenchymal Stem Cell Exosomes Alleviates Parkinson's Disease. Neuroscience. 2024;549:1-12.

[26] Wang CC, Hu XM, Long YF, et al. Treatment of Parkinson's disease model with human umbilical cord mesenchymal stem cell-derived exosomes loaded with BDNF. Life Sci. 2024;356:123014.

[27] Zhang Y, Zhang F, Yin H, et al. hUC-MSC-derived exosomes ameliorate Alzheimer's disease pathology through lncRNA-9969-mediated multi-target

protection involving neuronal autophagy and microglial modulation. Alzheimers Res Ther. 2026;18(1):34.

[28] Ding M, Shen Y, Wang P, et al. Exosomes Isolated From Human Umbilical Cord Mesenchymal Stem Cells Alleviate Neuroinflammation and Reduce Amyloid-Beta Deposition by Modulating Microglial Activation in Alzheimer's Disease. Neurochem Res. 2018;43(11):2165-2177.

[29] Shen B, Chen J, Liu N, Hou J, Dai Y. Therapeutic mechanisms of umbilical cord mesenchymal stem cell-derived exosomes in ischemic stroke: A transcriptomic and metabolomic study. Neural Regen Res. 2026;21(6):2632-2642.

[30] Sun Y, Zhao J, Liu Q, et al. Intranasal delivery of small extracellular vesicles from specific subpopulation of mesenchymal stem cells mitigates traumatic spinal cord injury. J Control Release. 2024;369:335-350.

[31] Sun Y, Zhao J, Liu Q, et al. Intranasal delivery of small extracellular vesicles from specific subpopulation of mesenchymal stem cells mitigates traumatic spinal cord injury. J Control Release. 2024;369:335-350.

[32] Sánchez SV, Otavalo GN, Gazeau F, Silva AKA, Morales JO. Intranasal delivery of extracellular vesicles: A promising new approach for treating neurological and respiratory disorders. J Control Release. 2025;379:489-523.

[33] Gotoh S, Kawabori M, Fujimura M. Intranasal administration of stem cell-derived exosomes for central nervous system diseases. Neural Regen Res. 2024;19(6):1249-1255.

[34] Prodromos CC, Del Villar R, Striegel A, Pena G, Dixit R. The Molecular Basis of Partial Reversal or Significant Slowing of ALS, Parkinson's Disease, and Lewy Body Dementia by Mesenchymal Exosomes/Secretome. Int J Mol Sci. 2026;27(10):4483.

[35] Goutman SA, Hardiman O, Al-Chalabi A, et al. Emerging insights into the complex genetics and pathophysiology of amyotrophic lateral sclerosis. Lancet Neurol. 2022;21(5):465-479.

[36] Tzeplaeff L, Wilfling S, Requardt MV, Herdick M. Current State and Future Directions in the Therapy of ALS. Cells. 2023;12(11):1523.

[37] Giunti D, Marini C, Parodi B, et al. Role of miRNAs shuttled by mesenchymal stem cell-derived small extracellular vesicles in modulating neuroinflammation. Sci Rep. 2021;11(1):1740.

[38] Tolomeo AM, Zuccolotto G, Malvicini R, et al. Biodistribution of Intratracheal, Intranasal, and Intravenous Injections of Human Mesenchymal Stromal Cell-Derived Extracellular Vesicles in a Mouse Model for Drug Delivery Studies. Pharmaceutics. 2023;15(2):548.

[39] Hirota R, Lankford KL, Nakazaki M, Toyoshima M, Kocsis JD. Intranasal administration of human mesenchymal stromal cell-derived small extracellular vesicles delays disease progression in the SOD1(G93A) mouse model. Mol Brain. 2026;19(1):22.

[40] Shen W, You T, Xu W, Xie Y, Wang Y, Cui M. Rapid and Widespread Distribution of Intranasal Small Extracellular Vesicles Derived from

Mesenchymal Stem Cells throughout the Brain Potentially via the Perivascular Pathway. Pharmaceutics. 2023;15(11):2578.

[41] Zhao J, Yang J, Jiao J, Wang X, Zhao Y, Zhang L. Biomedical applications of artificial exosomes for intranasal drug delivery. Front Bioeng Biotechnol. 2023;11:1271489.

[42] Turano E, Scambi I, Virla F, Bonetti B, Mariotti R. Extracellular Vesicles from Mesenchymal Stem Cells: Towards Novel Therapeutic Strategies for Neurodegenerative Diseases. Int J Mol Sci. 2023;24(3):2917.

[43] Susa F, Limongi T, Borgione F, et al. Comparative Studies of Different Preservation Methods and Relative Freeze-Drying Formulations for Extracellular Vesicle Pharmaceutical Applications. ACS Biomater Sci Eng. 2023;9(10):5871-5885.

[44] Trenkenschuh E, Richter M, Heinrich E, Koch M, Fuhrmann G, Friess W. Enhancing the Stabilization Potential of Lyophilization for Extracellular Vesicles. Adv Healthc Mater. 2022;11(5):e2100538.

[45] Verma S, Khurana S, Vats A, et al. Neuromuscular Junction Dysfunction in Amyotrophic Lateral Sclerosis. Mol Neurobiol. 2022;59(3):1502-1527.

[46] Wang XX, Chen WZ, Li C, Xu RS. Current potential pathogenic mechanisms of copper-zinc superoxide dismutase 1 (SOD1) in amyotrophic lateral sclerosis. Rev Neurosci. 2024;35(5):549-563.

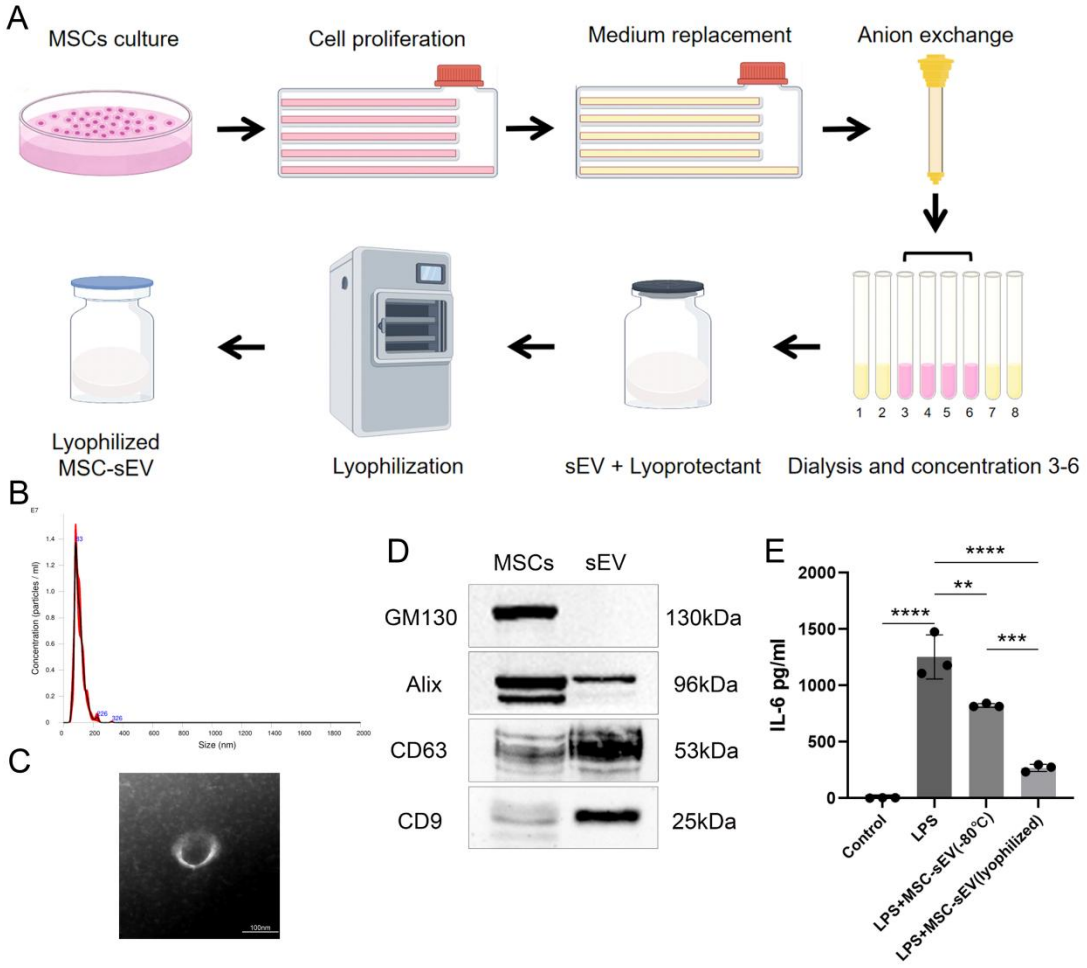
[47] Ciuro M, Sangiorgio M, Leanza G, Gulino R. Neuroinflammation and Oxidative Stress in SOD1 Animal Models of ALS: A Meta-analysis Study of

Their Effects on Disease Onset and Progression. Mol Neurobiol. 2026;63(1):477.

[48] Kreutzer FP, Meinecke A, Schmidt K, Fiedler J, Thum T. Alternative strategies in cardiac preclinical research and new clinical trial formats. Cardiovasc Res. 2022;118(3):746-762.

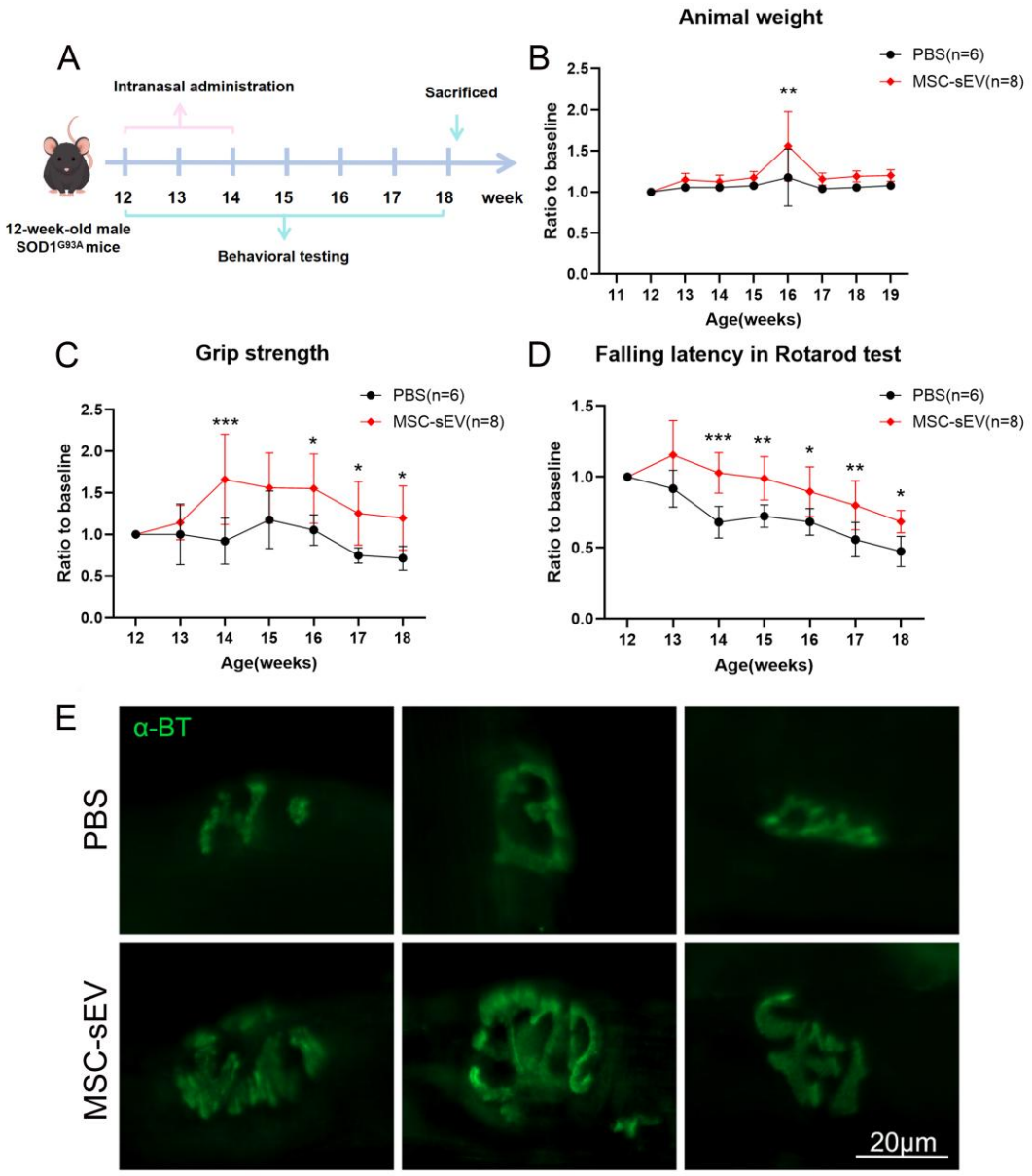
Figure Legends

Figure 1. Extraction and characterization of MSC-sEVs.



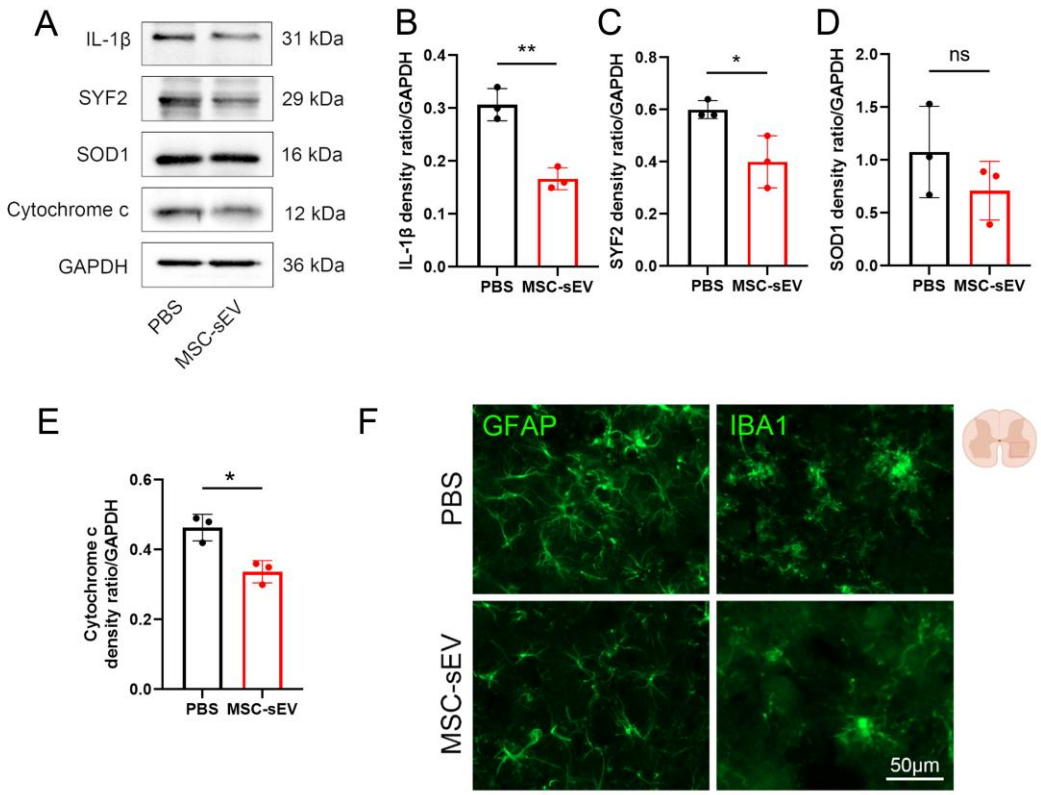
A. The preparation process of sEVs. B. NTA detection of sEVs. C. The transmission electron microscopy images of sEVs. D. Western blot identification diagram. E. ELISA statistical analysis graph of IL6 level. Data are mean ± SD. **P < 0.01; ***P < 0.001; ****P < 0.0001.

Figure 2. Improvement of motor function in SOD1^{G93A} transgenic mice by intranasal delivery of MSC-sEVs.



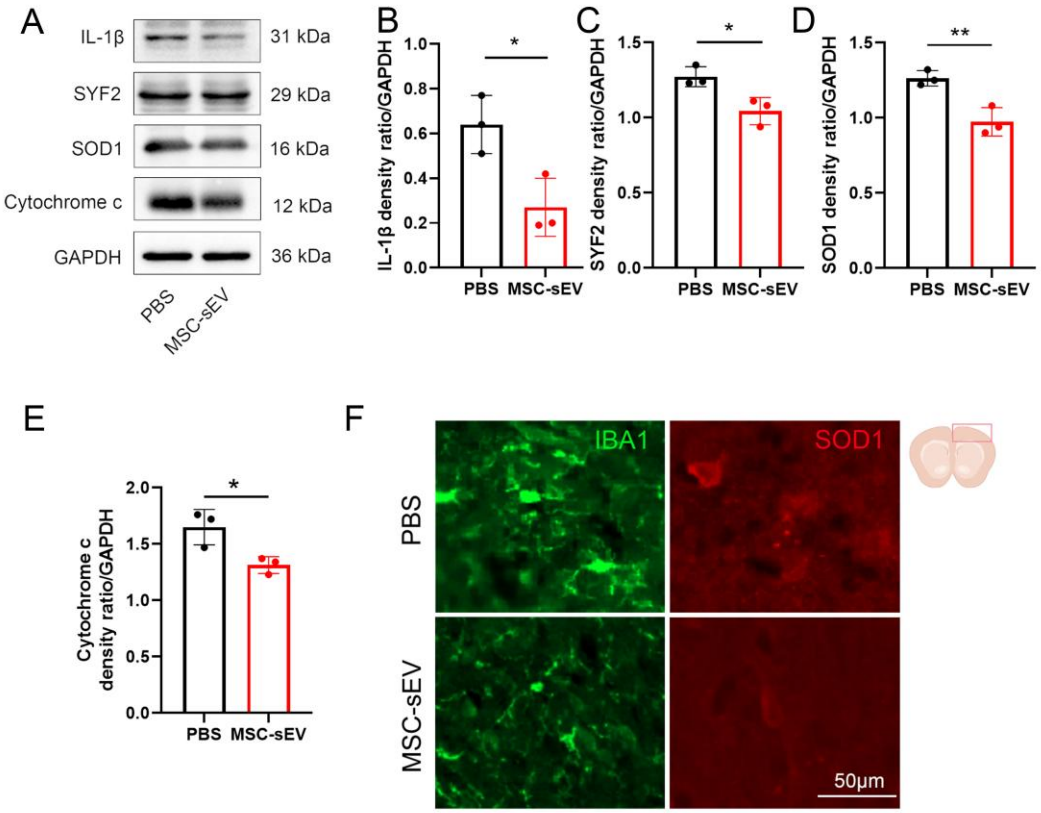
A. Experimental flowchart of SOD1^{G93A} transgenic mice. B. Line graph of weekly body weight ratio of SOD1^{G93A} mice compared to baseline. C. Weekly grip strength ratio of SOD1^{G93A} transgenic mice. D. Weekly rod-turning latency ratio of SOD1^{G93A} transgenic mice. E. α-BT immunofluorescence staining of gastrocnemius muscle of SOD1^{G93A} transgenic mice. Data are mean ± SD. *P < 0.05; **P < 0.01; ***P < 0.001.

Fig. 3. Intranasal delivery of MSC-sEVs improves spinal nerve inflammation in SOD1^{G93A} transgenic mice.



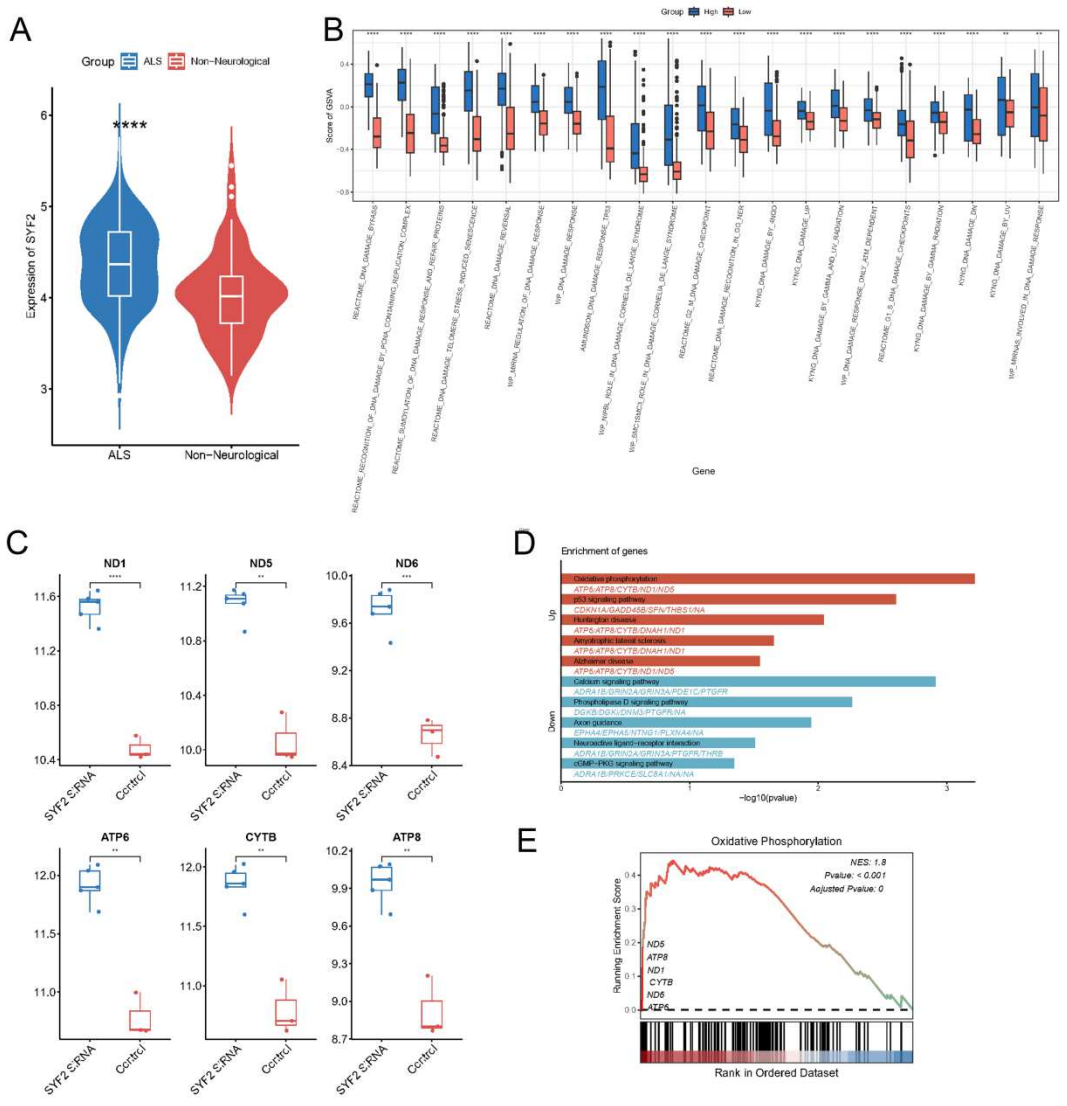
A. Protein bands of IL-1β, SYF2, SOD1, and Cytochrome C in the spinal cord of SOD1^{G93A} transgenic mice. B-E. Statistical analysis graphs of IL-1β, SYF2, SOD1, and Cytochrome C protein bands. F. Immunofluorescence staining images of GFAP and IBA1 in the spinal cord of SOD1^{G93A} transgenic mice. Data are mean ± SD. *P < 0.05; **P < 0.01.

Fig. 4. Intranasal delivery of MSC-sEVs improves neuroinflammation in the cerebral cortex of SOD1^{G93A} transgenic mice.



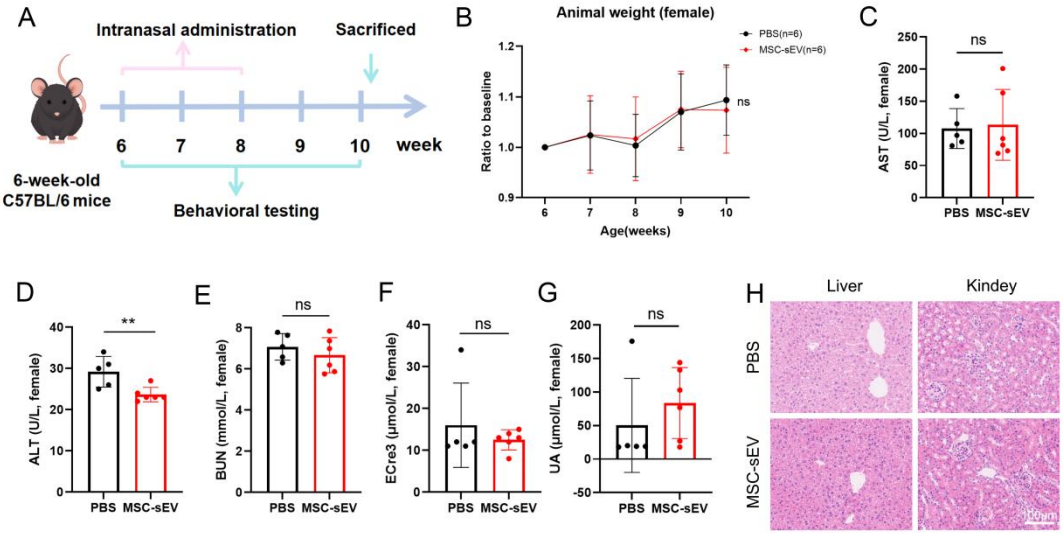
A. Protein bands of IL-1β, SYF2, SOD1, and Cytochrome C in the cerebral cortex of SOD1^{G93A} transgenic mice. B-E. Statistical analysis graphs of the protein bands of IL-1β, SYF2, SOD1, and Cytochrome C. F. IBA1 and SOD1 immunofluorescence staining images of the cerebral cortex of SOD1^{G93A} transgenic mice. Data are mean ± SD. *P < 0.05; **P < 0.01.

Figure 5. SYF2 is closely related to the progression of ALS disease.



A. The gene expression box diagram shows that the expression of SYF2 is significantly upregulated in ALS patients. B. The scores of multiple DNA damage-related signaling pathways are upregulated in the high-expression SYF2 group. C. After silencing SYF2, the expressions of mitochondrial genes ND1, ND5, ATP6, ND6, CYTB, and ATP8 are upregulated. D-E. Pathway enrichment analysis indicates that the upregulated genes after SYF2 silencing are mainly enriched in the oxidative phosphorylation pathway and various neurological disease pathways.

753 Figure 6. Safety evaluation of MSC-sEVs in female mice.

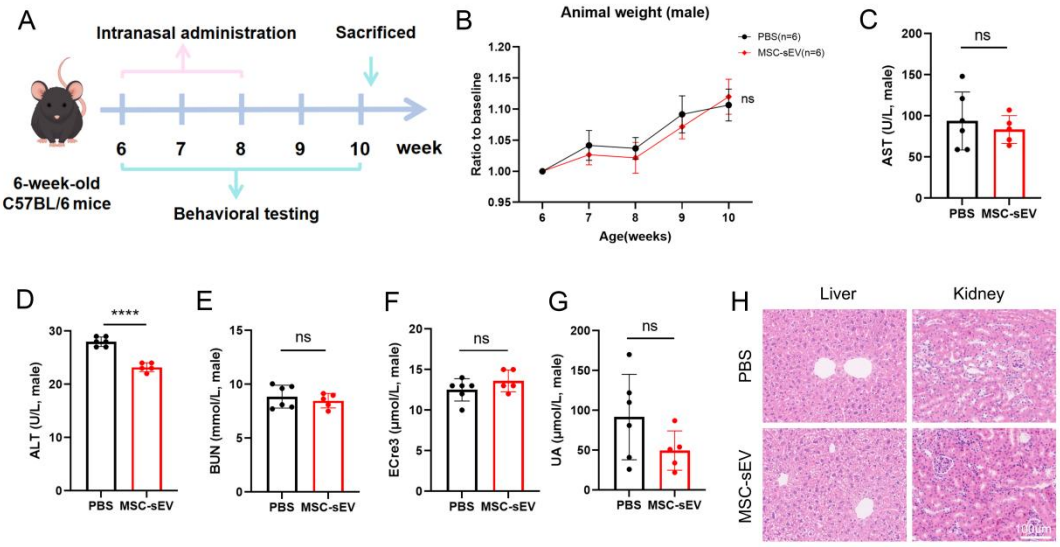


754

755 A. Flowchart of the safety experiment on female mice. B. Line graph showing the
756 weekly weight-to-baseline ratio of female mice. C. The level of AST in the serum of
757 female mice. D. The level of ALT in the serum of female mice. E. The level of BUN in
758 the serum of female mice. F. The level of ECre3 in the serum of female mice. G. The
759 level of UA in the serum of female mice. H. HE staining of liver and kidney in female
760 mice. Data are mean ± SD. ** $P < 0.01$.

761

762 Figure 7. Safety evaluation of MSC-sEVs in male mice.



763

764 A. Flowchart of the safety experiment on male mice. B. Line graph showing the weekly
765 weight-to-baseline ratio of male mice. C. The level of AST in the serum of male mice.
766 D. The level of ALT in the serum of male mice. E. The level of BUN in the serum of
767 male mice. F. The level of ECre3 in the serum of male mice. G. The level of UA in the
768 serum of male mice. H. HE staining of liver and kidney in male mice. Data are mean ±
769 SD. **** $P < 0.0001$.